

Absorption of Light in a Single-Nanowire Silicon Solar Cell Decorated with an Octahedral Silver Nanocrystal

Sarah Brittman,^{†,‡,||} Hanwei Gao,^{†,‡,||} Erik C. Garnett,[§] and Peidong Yang^{*,†,‡}

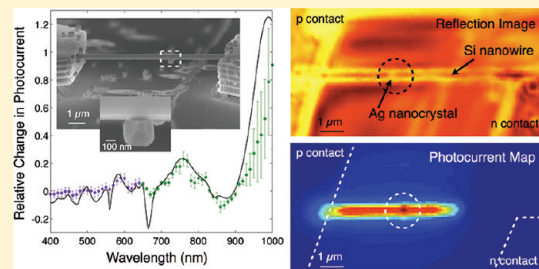
[†]Department of Chemistry, University of California, Berkeley, California 94720, United States

[‡]Materials Science Division, Lawrence Berkeley National Laboratory, 1 Cyclotron Road, Berkeley, California 94720, United States

[§]Department of Materials Science and Engineering, Stanford University, Stanford, California 94305, United States

Supporting Information

ABSTRACT: In recent photovoltaic research, nanomaterials have offered two new approaches for trapping light within solar cells to increase their absorption: nanostructuring the absorbing semiconductor and using metallic nanostructures to couple light into the absorbing layer. This work combines these two approaches by decorating a single-nanowire silicon solar cell with an octahedral silver nanocrystal. Wavelength-dependent photocurrent measurements and finite-difference time domain simulations show that increases in photocurrent arise at wavelengths corresponding to the nanocrystal's surface plasmon resonances, while decreases occur at wavelengths corresponding to optical resonances of the nanowire. Scanning photocurrent mapping with submicrometer spatial resolution experimentally confirms that changes in the device's photocurrent come from the silver nanocrystal. These results demonstrate that understanding the interactions between nanoscale absorbers and plasmonic nanostructures is essential to optimizing the efficiency of nanostructured solar cells.



KEYWORDS: Nanowire, solar cell, photovoltaics, plasmonics, nanocrystal

Photovoltaic conversion of sunlight to electricity is a promising and proven technology for large-scale production of energy from a renewable source.^{1,2} To generate electricity efficiently, however, a photovoltaic cell must absorb most of the solar spectrum as well as collect the photogenerated carriers with minimal losses to recombination. For planar solar cells, this combined task can be difficult because the thickness of material required for adequate absorption of light is often greater than the distance over which photogenerated charges can be efficiently collected.

Semiconductor nanostructures offer new approaches to meet these requirements for absorption and charge collection.³ Because of their ability to scatter and trap incident light, arrays of vertically aligned micro- and nanowires absorb more light than their planar counterparts,^{4–7} while individual nanowires support optical resonances that can increase their absorption at various wavelengths.^{8–10} Additionally, a core–shell wire geometry allows absorption of light over the full length of the wire while maintaining the wire's much smaller radius as the relevant distance for charge collection.¹¹ As all of these effects arise from the geometry of nanowires, such nanostructuring offers a way to improve a material's absorption without modifying its composition.

Metal nanostructures also offer intriguing possibilities for increasing absorption of light in poorly absorbing materials. At a metal's surface, collective oscillations of the free electrons produce excitations known as surface plasmons. The resonance frequencies of these plasmons depend sensitively on the metal's free electron density and band structure, the nanostructure's size

and geometry, and the local dielectric environment.^{7,12–15} Excitation of surface plasmons by incident light leads to intense evanescent electric fields at the nanostructure's surface, particularly at sharp edges and points,^{16,17} as well as to enhanced scattering and absorption cross sections.¹⁸ Both evanescent and scattered fields can yield increased absorption of light within the surrounding dielectric media,^{19–22} which then leads to higher energy conversion efficiencies in solar cells.^{23–28} Since the plasmonic properties of metal nanostructures are tunable throughout the visible and near-infrared regions of the spectrum,^{7,29} they offer another way to modify the absorption of a solar material without changing its composition.

In either approach used to improve absorption, nanostructuring the dielectric solar material or coupling it to metal nanostructures, light interacts with subwavelength features. In this work, a silicon single-nanowire solar cell decorated with an octahedral silver nanocrystal combines these two approaches, and the nanocrystal modifies the nanowire's photocurrent in a highly wavelength-dependent manner. Three-dimensional finite-difference time domain (FDTD) simulations of the nanowire's absorption of light agree well with the experimental photocurrent measurements. The simulations show that increases in the photocurrent result from the surface plasmon resonances of the nanocrystal, while decreases occur at the wavelengths of the

Received: July 12, 2011

Revised: October 27, 2011

Published: November 14, 2011

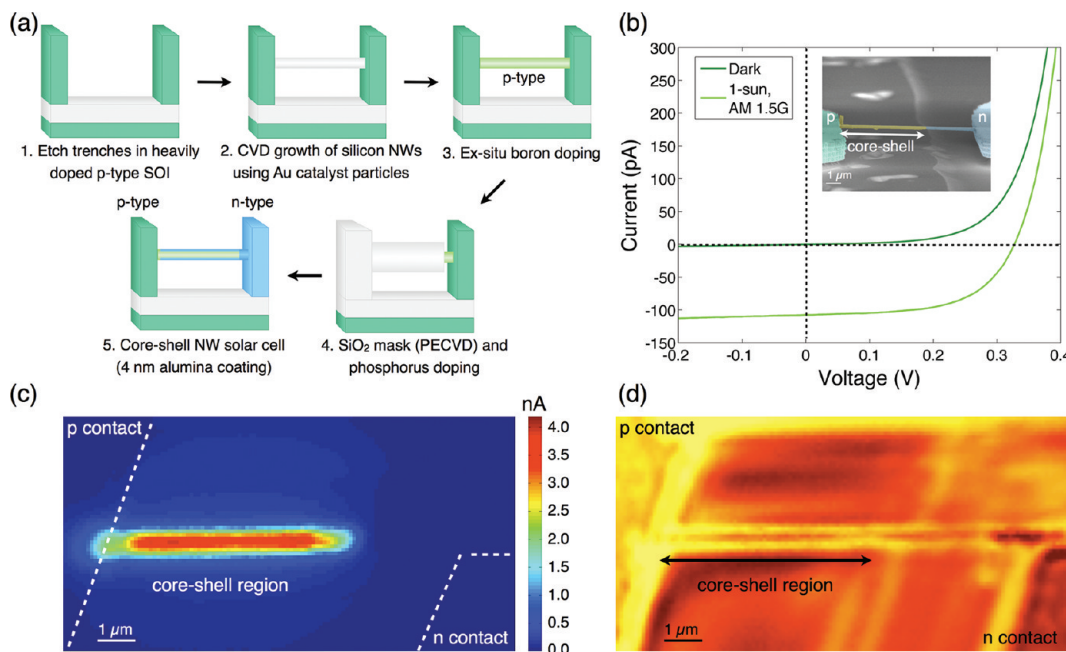


Figure 1. Fabrication scheme (a) and typical $I-V$ curve under simulated solar illumination (b) of a suspended silicon single-nanowire solar cell. The inset in (b) is a side view SEM image of a completed device with false coloring to denote the p (green) and n (blue) contacts and the core–shell region of the device (brown). Scanning photocurrent map of a single-nanowire solar cell (c) and its corresponding scanning optical image collected simultaneously (d). Lighter regions in the optical image correspond to regions of reduced reflection. The scans were taken at $\lambda = 442 \text{ nm}$, $P \sim 7 \text{ W/cm}^2$.

nanowire's optical resonances. Such insight into how the nanowire's absorption of light arises from the metal nanocrystal–nanowire interaction is essential to the design of efficient nanostructured solar cells.

Silicon single-nanowire solar cells suspended above the substrate were fabricated using chemical vapor deposition (CVD) and standard high-temperature doping processes (Figure 1a, details in Supporting Information). Briefly, trenches were etched to the buried oxide layer in heavily doped p-type silicon-on-insulator (SOI). Using gold colloids as catalysts for one-dimensional growth, silicon nanowires were grown to bridge the trenches above the substrate.³⁰ The wires were then doped p-type with boron in a gas-phase reaction and subsequently masked with silicon dioxide deposited using plasma-enhanced chemical vapor deposition (PECVD). Photolithography and wet etching removed the mask from one end of the nanowires and one of their contacts, and the rectifying junction was formed by n-type vapor-phase doping with phosphorus. The PECVD-deposited oxide mask was permeable to the phosphorus dopant, but the difference in the thickness of the mask on each wire and its unexposed contact resulted in a core–shell p–n junction in only the wire, as confirmed by scanning photocurrent mapping, discussed below. After removal of the mask, the devices were coated with 4 nm of aluminum oxide deposited by atomic layer deposition to serve both as a surface passivation layer and later as a dielectric spacer between the nanowire solar cells and the octahedral silver nanocrystals. A false-color scanning electron microscopy (SEM) image of a typical finished device denotes the p-type contact, the core–shell region of the nanowire, the fully n-type region of nanowire, and the n-type contact (inset, Figure 1b).

Current–voltage ($I-V$) measurements and scanning photocurrent mapping confirmed that individual nanowires functioned as solar cells. Measured under simulated 1-sun, AM 1.5G illumination,

the $I-V$ curve for a typical device (Figure 1b) shows a short-circuit current of 108 pA, an open-circuit voltage of 0.32 V, and a fill factor of 0.59. Scanning photocurrent mapping was used to visualize the active region of individual devices. By comparing the scanning photocurrent map (Figure 1c) and the optical image obtained simultaneously (Figure 1d), it is clear that only the core–shell region of the nanowire is active, not the n-type region or either of the contacts. The inactivity of the n-type side of the nanowire results from a short minority carrier diffusion length in that region, which is consistent with the high doping level expected from the phosphorus doping reaction. The uniform photocurrent along the length of the wire that shows no decay indicates that the junction is core–shell. While such uniform photocurrent would also appear if the minority carrier diffusion length were much longer than the nanowire's physical length, scanning photocurrent mapping of axial junctions produced by shortening the phosphorus diffusion time indicates that the minority carrier diffusion length within the nanowire is less than 1 μm (Supporting Information, Figure S1).

Experimental measurements and numerical simulations show that the nanowire solar cell exhibits peaks in its photocurrent at wavelengths corresponding to the wire's optical resonances. The spectrally resolved short-circuit current, normalized to the incident photon flux, is shown for a nanowire with a diameter of 288 nm (Figure 2a). Because silicon absorbs weakly in the red and near-infrared wavelengths,³¹ the experimental setup was modified slightly (Supporting Information) to measure these wavelengths; therefore, the short (Figure 2a) and long wavelength (Figure 2b) data appear separately. Error bars reflect the precision of the experimental setup and were calculated from one standard deviation of six replicated photocurrent measurements taken at every wavelength on the same device. While the absorption coefficient of silicon decreases monotonically

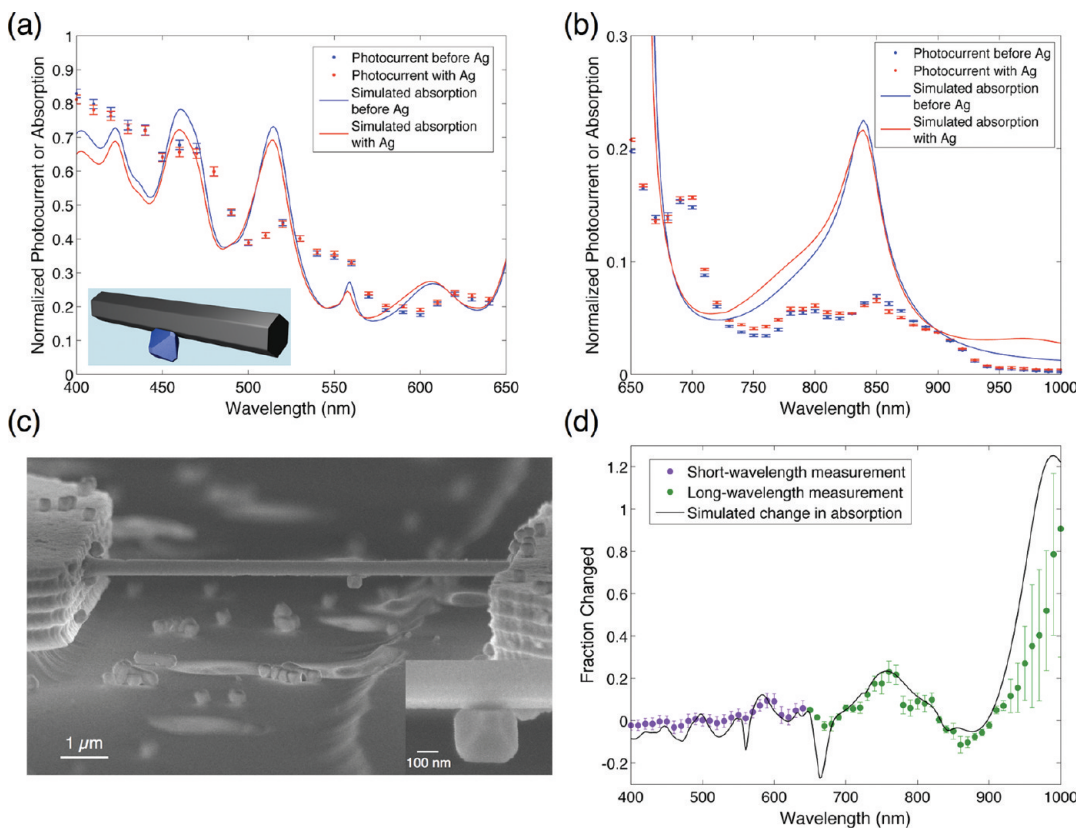


Figure 2. Measured photocurrent spectra of a single-nanowire solar cell (288 nm diameter) without (blue) and with (red) a single silver octahedron in the 400–650 nm (a) and 650–1000 nm (b) regions. Three-dimensional FDTD simulations of absorption within the wire without (blue) and with (red) the silver octahedron are overlaid onto the experimental plots. The inset in (a) shows the simulated geometry as determined by side view SEM images of the device (c, inset). Error bars on the experimental measurements reflect the precision of the experimental setup. The change in photocurrent caused by the silver octahedron, relative to its initial value, was extracted from (a) and (b) and plotted in (d) along with the change predicted by the simulation (black).

throughout this wavelength region,³¹ the silicon nanowire solar cell exhibits many small peaks in its photocurrent spectrum (Figure 2a,b). A three-dimensional FDTD simulation of the hexagonally faceted nanowire under illumination was used to calculate the nanowire's absorption. The results are superimposed on the experimental photocurrent data (Figure 2a,b). Clear peaks appear in the nanowire's simulated absorption spectrum and correspond to optical modes within the nanowire that are determined by its geometry, an effect that has been characterized well in germanium and silicon nanowires.^{8,9} The peaks in the experimental spectrum are less well defined than those in the simulation likely because the nanowire in the experiment was tapered. Two-dimensional FDTD simulations predict that the wavelengths of the optical modes in a silicon nanowire are highly sensitive to its diameter (Supporting Information, Figure S2a). Although the nanowire's diameter changes by only 20 nm over 9.5 μm, this tapering broadens the wire's optical resonances, which causes closely spaced peaks, such as those in the blue region of the spectrum, to merge (Supporting Information, Figure S2b). Since the nanowire solar cell has a core–shell junction, the device's internal quantum efficiency should be nearly constant for all wavelengths^{4,11} so that the photocurrent spectrum reflects differences in the nanowire's absorption at each wavelength. The nanowire devices responded linearly to changes in light intensity (Supporting Information, Figure S3), indicating that any changes

in photocurrent were directly proportional to their absorption of light.

Immediately following characterization of the nanowire solar cells, octahedral silver nanocrystals were deposited onto the devices. The nanocrystals, whose edges measured about 270 nm, were synthesized by the polyol method using poly(vinyl pyrrolidone) (PVP) as the shape-controlling agent.³² Capped in PVP, the nanocrystals were suspended in ethanol and drop cast onto the devices. After allowing the ethanol to dry, the devices were rinsed in isopropanol and blown dry with nitrogen. Because of the solution's low concentration, typically only a single nanocrystal was deposited onto an individual nanowire. Most often, the nanocrystal adhered to the facet on the wire's underside (Figure 2c). Following the addition of the silver nanocrystal, the short-circuit current was remeasured, and FDTD simulations using the geometry shown in the inset of Figure 2a were used to calculate the wavelength-dependent absorption of the nanowire decorated with the nanocrystal (Figure 2a,b).

Plotting the relative change in photocurrent at each wavelength reveals the highly wavelength-dependent effect of the silver nanocrystal (Figure 2d). The experimental changes in photocurrent are in excellent agreement with those predicted by the FDTD simulation, demonstrating that the simulation does capture the relevant interactions between light and the nanocrystal–nanowire structure. Notable features include the two broad peaks in enhancement centered at 981 and 750 nm, as well

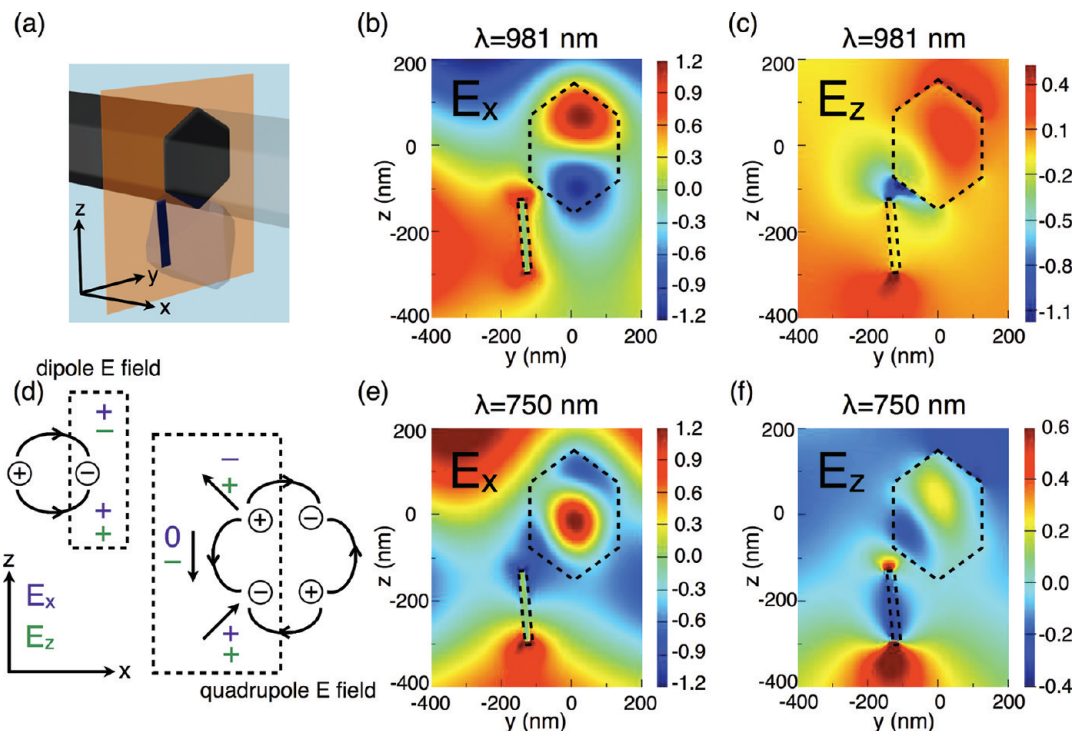


Figure 3. Geometry of the plane of the simulated field plots in which the cross-sectional plane slices the edge of the octahedron (a). In the following plots, dashed lines outline the octahedron's rectangular edge and the nanowire's hexagonal cross section. The nanowire and octahedron were simulated as being illuminated by an x -polarized plane wave propagating in the negative z -direction. Simulated E_x (b) and E_z (c) in the $y-z$ plane at the octahedron's edge at $\lambda = 981$ nm. The unchanged phase of E_x and the changing phase of E_z in the z -direction indicate that the octahedron exhibits a dipolar resonance along the x -direction (d, top left). Black arrows in (d) indicate the electric field lines with the phases of E_x (purple) and E_z (green) labeled. Because the simulation plane is cut at the edge of the octahedron, only the field components in the dashed boxes are visible. Simulated E_x (e) and E_z (f) in the $y-z$ plane at the octahedron's edge at $\lambda = 750$ nm. The changing phase of E_x and the changing phase of E_z in the z -direction indicate that the octahedron exhibits a quadrupolar resonance in the $x-z$ plane (d, bottom right). Magnitudes of the field components are in arbitrary units.

as the several dips in absorption that occur at wavelengths corresponding to the nanowire's optical resonances. Although the experimental photocurrent spectra were measured using unpolarized light, the origin of these features can be better understood by studying the simulated polarization-dependent electric field distributions at the relevant wavelengths.

By considering the electric field distribution of the system when illuminated by light polarized along the wire's axis, the two broad peaks in enhancement centered at 981 and 750 nm can be attributed to the nanocrystal's predominantly dipolar and quadrupolar surface plasmon resonances, respectively. The geometry of the simulation is shown in Figure 3a, in which the cross-sectional plane slices the edge of the octahedron. When the particle and wire are excited by light propagating in the negative z -direction and polarized in the x -direction, the phase of the x -component of the electric field (E_x) at the edge of the octahedron does not change in the direction of propagation, while the phase of the z -component (E_z) does change sign (Figure 3a,b). This field orientation at the edge of the nanocrystal is consistent with the expected electric field of a dipole surface plasmon resonance (Figure 3c). At 750 nm, the phase of E_x changes once and the phase of the E_z changes twice, which is consistent with the particle's quadrupolar resonance (Figure 3c–e). Since the light is polarized parallel to the long axis of the nanowire, the silver octahedron's charge oscillations are perturbed uniformly along their path by the nearby dielectric; consequently, the optical response reflects the free-space resonances of the nanocrystal but shifted to longer wavelengths by the polarizability of the local

dielectric (Supporting Information, Figure S4). This excitation and its result are analogous to the common experimental geometry in which a metal nanocrystal sitting on a dielectric substrate is excited with light that is incident normal to the substrate.^{14,33,34}

In contrast, when the light is polarized along the y -direction, the dielectric of the wire perturbs the charge oscillations asymmetrically along their path. The geometry of this simulation is shown in Figure 4a, in which the cross-sectional plane slices through the center of the octahedron. At 981 nm, the several lobes surrounding the nanocrystal in both E_y and E_z suggest that the strong interaction between the particle and the wire causes the charge oscillations to dephase, and the resonance takes on some quadrupole character (Figure 4b,c). The absorption peak of the nanocrystal–nanowire system for this polarization is blue shifted from the same peak for x -polarized illumination, as expected for the mixing of the dipole and quadrupole resonances (Figure 4d). At 750 nm, similar nodal symmetry appears in the E_y and E_z field components (Figure 4e,f), although the lobes are more pronounced. This enhancement peak has red shifted from its position for x -polarized illumination (Figure 4d), suggesting that it too now reflects a mixture of the particle's dipole and quadrupole resonances. From both the y -polarized and x -polarized field plots, it is clear that the solar cell's increased photocurrent arises because the silver octahedron's surface plasmon resonances couple light into the wire.

A third notable feature in the photocurrent spectrum is the sharp decrease in photocurrent near 660 nm. For x -polarized light, the wire exhibits a whispering gallery resonance at 661 nm

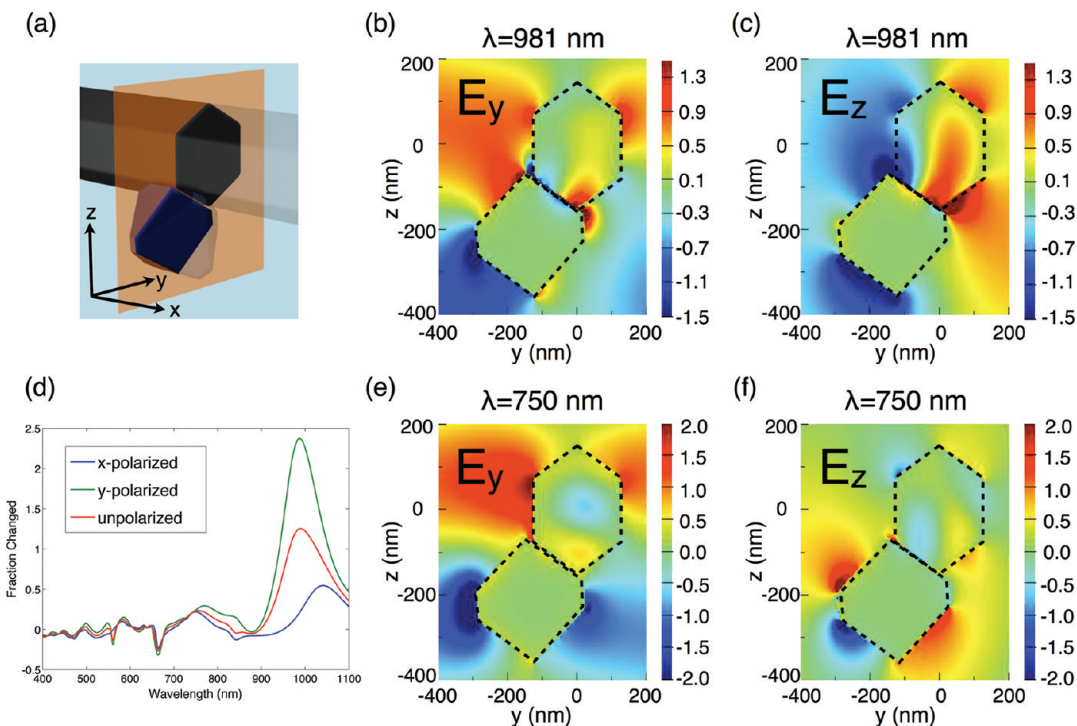


Figure 4. Geometry of the plane of the simulated field plots in which the cross-sectional plane slices through the center of the octahedron (a). In the following plots, dashed lines outline the cross sections of the octahedron and the nanowire. The nanowire and octahedron were simulated as being illuminated by a *y*-polarized plane wave propagating in the negative *z*-direction. Simulated E_y (b) and E_z (c) in the *y*-*z* plane at the octahedron's center at $\lambda = 981$ nm. The node in E_y at the nanocrystal's surface suggests that the resonance has partial quadrupole character. (d) Simulated change in the nanowire's absorption for unpolarized (red), *y*-polarized (green), and *x*-polarized (blue) illumination showing the dependence of the peak positions on polarization. Simulated E_y (e) and E_z (f) in the *y*-*z* plane at the octahedron's center at $\lambda = 750$ nm. The similar symmetry also suggests quadrupole character. Magnitudes of the field components are in arbitrary units.

at distances far from the nano-octahedron (Figure 5a). Closer to the nanocrystal (Figure 5b,c), this resonance becomes distorted and the field within the nanowire decreases, indicating that the absorption in the wire is reduced locally because of the nanocrystal. Under *y*-polarized illumination, a Fabry-Pérot resonance exists in the wire at 657 nm, which is also locally perturbed by the octahedron (Figure 5d–f), causing a reduction in absorption. This decreased absorption at an optical mode of the solar cell has been predicted theoretically^{35,36} and observed experimentally²⁶ in nanoscale thin-film solar cells that support propagating modes. Such decreases are not expected, however, when the design of the solar cell isolates the absorbing material from the plasmonic metal structures with a relatively thick (~ 10 nm) dielectric layer.^{37,38} Since the octahedral nanocrystal does not exhibit a resonance near 660 nm, the local disruption of the nanowire's modes arises from its geometric perturbation of the wire and is expected to occur for any other such perturbation, such as a dielectric particle or notch in the nanowire.

Scanning photocurrent mapping experimentally confirms that changes in the device's photocurrent do arise from the position of the nanocrystal. Before the addition of the nanocrystal, the nanowire displays uniform photocurrent throughout its active area (Figure 1c). With the addition of the nanocrystal to the underside of the wire, the photocurrent map shows a localized increase in photocurrent at the position of the particle (Figure 6a) and a point of reduced reflection appears in the scanning optical image (Figure 6b). The small photocurrent enhancement at 442 nm is consistent with the FDTD-simulated increase in absorption for a nanowire of this size, 320 nm in

diameter (Figure 6c). The top and side view SEM images show the octahedron on the underside of the wire (Figure 6d and inset). The octahedron is clearly the source of the change in photocurrent, which is in agreement with similar measurements performed on silicon nanowire photodetectors;²² however, this measurement cannot distinguish between local field enhancement and far-field scattering effects since collection of the photocurrent is not localized. While numerical simulations show that some of the enhancement arises from near-field effects (Supporting Information, Figure S5), scanning photocurrent mapping suggests that some of the enhancement also arises from far-field scattering because nanocrystals situated on the inactive portion of the nanowire appear in the photocurrent maps (Supporting Information, Figure S6).

Because all of the reported results arise from a single nanocrystal on the solar cell's active region that measures about $6.6 \mu\text{m}$ in length, each additional isolated nanocrystal on the wire's underside is expected to create a comparable change in the device's photocurrent. If the nanocrystals were close enough to couple to each other, however, the surface plasmon resonances would change,³⁹ and interactions between the wire and these new resonances would have to be considered. As demonstrated in the case of a single nanocrystal, new resonances at wavelengths far from the nanowire's modes would enhance the photocurrent, but the case in which the resonances of the nanowire and plasmonic particles occur at the same wavelength requires further study. Additionally, since the wavelengths of the nanowire's resonances can be tuned by changing the wire's diameter and the nanocrystal's resonances

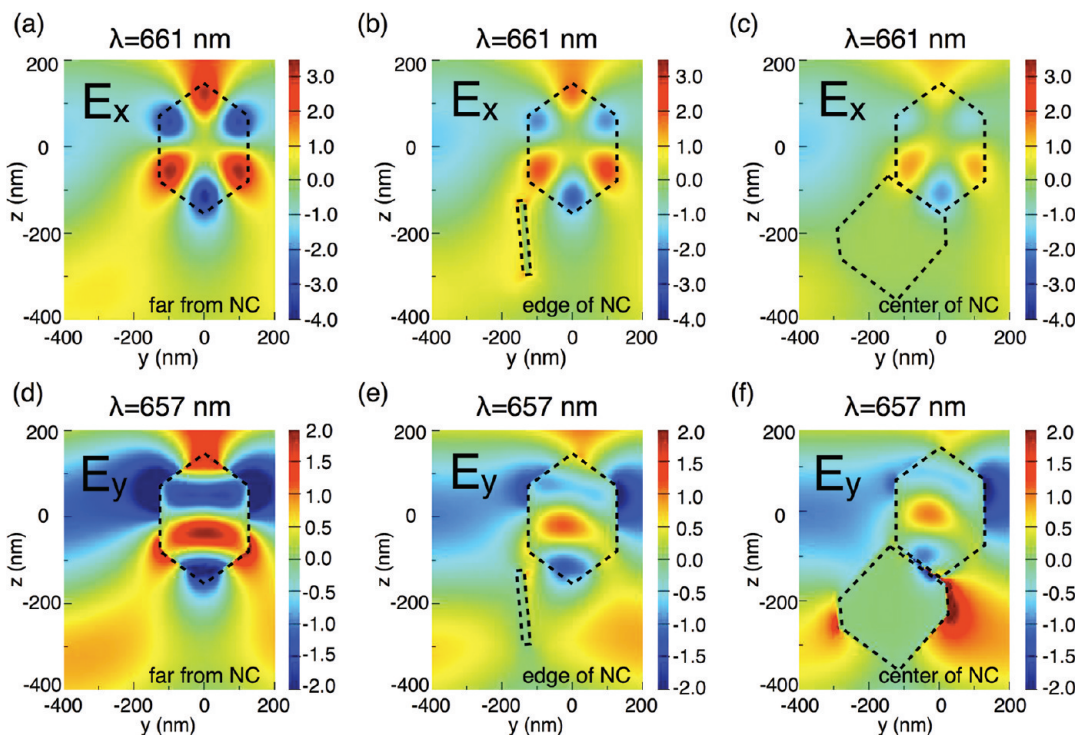


Figure 5. E_x in the $y-z$ plane under x -polarized illumination of $\lambda = 661 \text{ nm}$ at positions along the wire of 700 nm (a), 140 nm (b), and 0 nm (c) from the center of the octahedral nanocrystal (NC) showing the local perturbation of the nanowire's whispering gallery mode. E_y (d,e,f) under y -polarized illumination of $\lambda = 657 \text{ nm}$ at positions along the wire of 700 (d), 140 (e), and 0 nm (f) from the octahedron's center showing the local perturbation of the nanowire's Fabry-Pérot mode. Magnitudes of the field components are in arbitrary units.

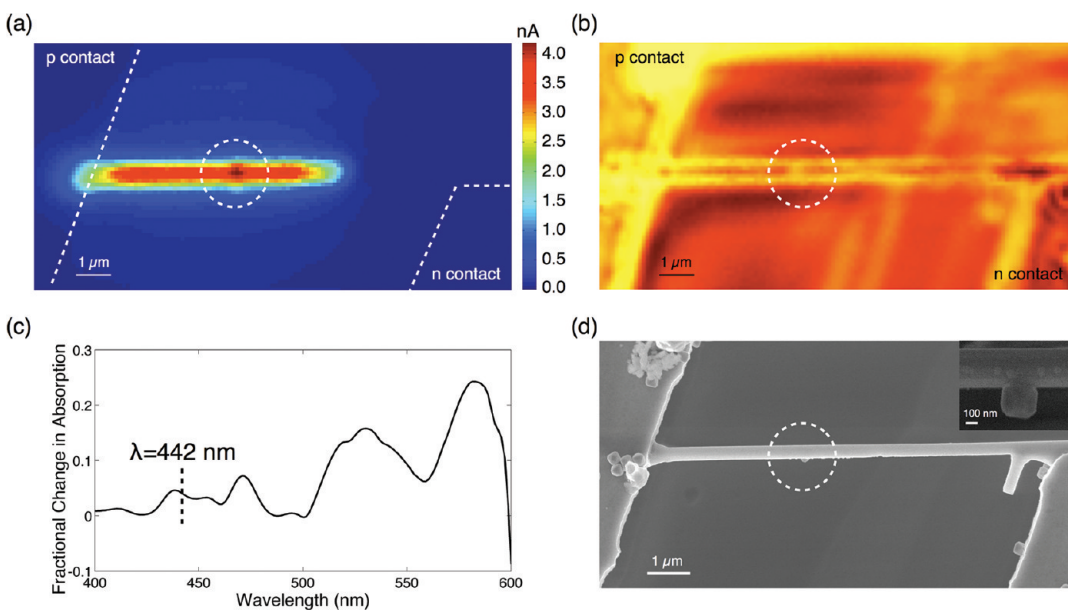


Figure 6. Scanning photocurrent map (a) of the single-nanowire solar cell (320 nm diameter) shown in Figure 1a,b after the addition of a silver octahedron. Corresponding scanning optical image collected simultaneously showing the scattering at the position of the octahedron (b). Each scan is approximately $12.6 \mu\text{m} \times 6.3 \mu\text{m}$. The scans were taken with $\lambda = 442 \text{ nm}$, $P \sim 7 \text{ W/cm}^2$. The enhancement in photocurrent is localized to the position of the silver octahedron and is consistent with the enhancement in absorption predicted by an FDTD simulation for a nanowire of this size (c). Top view SEM of the same device (d), and the inset is a side view SEM of the octahedron attached to the wire.

are sensitive to the particle's size and shape, much latitude exists for tailoring the interaction between the wire and nanocrystal to optimize enhancement of the photocurrent.

In conclusion, the wavelength-dependent effect of an octahedral silver nanocrystal on the absorption of a silicon nanowire solar cell has been quantified experimentally and interpreted

using FDTD simulations. Increases in the nanowire's absorption and photocurrent arise from the coupling of the nanocrystal's dipolar and quadrupolar resonances to the wire. Decreases occur at wavelengths for which the particle perturbs the resonances of the nanowire itself; consequently, when seeking to enhance the performance of nanostructured solar cells using plasmonic nanocrystals, care must be taken to ensure that the enhancements in photocurrent outweigh the losses. For isolated nanocrystals, simulations and scanning photocurrent mapping indicate that the observed increases in photocurrent do arise from the nanocrystal and result from both near-field interactions and far-field scattering. Clearly, when engineering light trapping using nanoscale absorbers and plasmonic nanostructures, understanding all the interactions between these structures is key to making efficient nanostructured solar cells.

■ ASSOCIATED CONTENT

Supporting Information. Detailed methods for fabrication of the nanowire solar cells, electrical and optical measurements, and FDTD simulations. Scanning photocurrent mapping of a single-nanowire solar cell with an axial junction. Two-dimensional numerical simulations of light absorption in a tapered silicon nanostructure. Dependence of a nanowire solar cell's short-circuit current on light intensity. Extinction spectrum of the silver octahedral nanocrystals suspended in ethanol. Numerical simulations of the increased electric field within the wire near the silver octahedron. Scanning photocurrent mapping of silver nanocrystals on the inactive region of the nanowire solar cell. This material is available free of charge via the Internet at <http://pubs.acs.org>.

■ AUTHOR INFORMATION

Corresponding Author

*E-mail: p_yang@berkeley.edu.

Author Contributions

^{||}These authors contributed equally to this work.

■ ACKNOWLEDGMENT

The authors thank Dr. Xing Yi Ling for synthesis of the octahedral silver nanocrystals, Dr. Daniel Gargas and Dr. Hung-Ta Wang for experimental assistance, and Dr. Jinyao Tang and Chong Liu for helpful discussions. Funding from the National Science Foundation Center of Integrated Nanomechanical Systems (NSF COINS) under Contract No. 0832819 is greatly appreciated.

■ REFERENCES

- (1) Price, S.; Margolis, R. 2008 *Solar Technologies Market Report*; U.S. Department of Energy: Washington, DC, 2010.
- (2) Little, R. G.; Collins, R. W.; Anderson, T.; Buller, B.; Dennler, G.; Gloeckler, M.; Karam, N. H.; Kurtz, S.; Olson, D. C.; Surek, T.; Wohlgemuth, J. *Foundations for Innovation: Photovoltaic Technologies for the 21st Century*; National Institute of Standards and Technology: Gaithersburg, MD, 2010.
- (3) Garnett, E.; Brongersma, M. L.; Cui, Y.; McGehee, M. D. *Ann. Rev. Mater. Res.* **2011**, *41*, 269–295.
- (4) Kelzenberg, M. D.; Boettcher, S. W.; Petykiewicz, J. A.; Turner-Evans, D. B.; Putnam, M. C.; Warren, E. L.; Spurgeon, J. M.; Briggs, R. M.; Lewis, N. S.; Atwater, H. A. *Nat. Mater.* **2010**, *9*, 239–244.
- (5) Garnett, E.; Yang, P. *Nano Lett.* **2010**, *10*, 1082–1087.
- (6) Yoon, H. P.; Yuwen, Y. A.; Kendrick, C. E.; Barber, G. D.; Podraza, N. J.; Redwing, J. M.; Mallouk, T. E.; Wronski, C. R.; Mayer, T. S. *Appl. Phys. Lett.* **2010**, *96*, 213503.
- (7) Zoric, I.; Zäch, M.; Kasemo, B.; Langhammer, C. *ACS Nano* **2011**, *5*, 2535–2546.
- (8) Cao, L.; White, J. S.; Park, J. S.; Schuller, J. A.; Clemens, B. M.; Brongersma, M. L. *Nat. Mater.* **2009**, *8*, 643–647.
- (9) Cao, L.; Fan, P.; Vasudev, A. P.; White, J. S.; Yu, Z.; Cai, W.; Schuller, J. A.; Fan, S.; Brongersma, M. L. *Nano Lett.* **2010**, *10*, 439–445.
- (10) Brönstrup, G.; Jahr, N.; Leiterer, C.; Csáki, A.; Fritzsche, W.; Christiansen, S. *ACS Nano* **2010**, *4*, 7113–7122.
- (11) Kayes, B. M.; Atwater, H. A.; Lewis, N. S. *J. Appl. Phys.* **2005**, *97*, 114302.
- (12) Maier, S. A.; Atwater, H. A. *J. Appl. Phys.* **2005**, *98*, 011101.
- (13) Langhammer, C.; Schwind, M.; Kasemo, B.; Zoric, I. *Nano Lett.* **2008**, *8*, 1461–1471.
- (14) Kelly, K. L.; Coronado, E.; Zhao, L. L.; Schatz, G. C. *J. Phys. Chem. B* **2003**, *107*, 668–677.
- (15) Bohren, C. F.; Huffman, D. R. *Absorption and Scattering of Light by Small Particles*; John Wiley & Sons: New York, 1983.
- (16) Gersten, J. I. *J. Chem. Phys.* **1980**, *72*, 5779.
- (17) Liao, P. F.; Wokaun, A. *J. Chem. Phys.* **1982**, *76*, 751.
- (18) Hao, E.; Schatz, G. C. *J. Chem. Phys.* **2004**, *120*, 357–366.
- (19) Atwater, H. A.; Polman, A. *Nat. Mater.* **2010**, *9*, 205–213.
- (20) Kulkarni, A. P.; Noone, K. M.; Munechika, K.; Guyer, S. R.; Ginger, D. S. *Nano Lett.* **2010**, *10*, 1501–1505.
- (21) Catchpole, K. R.; Polman, A. *Appl. Phys. Lett.* **2008**, *93*, 191113.
- (22) Hyun, J. K.; Lauhon, L. J. *Nano Lett.* **2011**, *11* (7), 2731–2734.
- (23) Pillai, S.; Catchpole, K. R.; Trupke, T.; Green, M. A. *J. Appl. Phys.* **2007**, *101*, 093105.
- (24) Yu, E. T.; Derkacs, D.; Matheu, P.; Schaadt, D. M. Plasmonic nanoparticle scattering for enhanced performance of photovoltaic and photodetector devices. *Proc. SPIE* **2008**, *7033*, 70331V.
- (25) Nakayama, K.; Tanabe, K.; Atwater, H. A. Surface plasmon enhanced photocurrent in thin GaAs solar cells. *Proc. SPIE* **2008**, *7047*, 704708.
- (26) Ferry, V. E.; Verschueren, M. A.; Li, H. B. T.; Verhagen, E.; Walters, R. J.; Schropp, R. E. I.; Atwater, H. A.; Polman, A. *Opt. Express* **2010**, *18*, A237–A245.
- (27) Beck, F. J.; Polman, A.; Catchpole, K. R. *J. Appl. Phys.* **2009**, *105*, 114310.
- (28) Wang, D. H.; Kim, D. Y.; Choi, K. W.; Seo, J. H.; Im, S. H.; Park, J. H.; Park, O. O.; Heeger, A. J. *Angew. Chem., Int. Ed.* **2011**, *50*, 5519–5523.
- (29) Tao, A.; Sinsermsuksakul, P.; Yang, P. *Angew. Chem., Int. Ed.* **2006**, *45*, 4597–4601.
- (30) He, R.; Gao, D.; Fan, R.; Hochbaum, A. I.; Carraro, C.; Maboudian, R.; Yang, P. *Adv. Mater.* **2005**, *17*, 2098–2102.
- (31) Green, M. A.; Keevers, M. J. *Prog. Photovoltaics* **1995**, *3*, 189–192.
- (32) Mulvihill, M. J.; Ling, X. Y.; Henzie, J.; Yang, P. *J. Am. Chem. Soc.* **2010**, *132*, 268–274.
- (33) Jensen, T. R.; Duval, M. L.; Kelly, K. L.; Lazarides, A. A.; Schatz, G. C.; Van Duyne, R. P. *J. Phys. Chem. B* **1999**, *103*, 9846–9853.
- (34) Sherry, L. J.; Chang, S. H.; Schatz, G. C.; Van Duyne, R. P.; Wiley, B. J.; Xia, Y. *Nano Lett.* **2005**, *5*, 2034–2038.
- (35) Ferry, V. E.; Sweatlock, L. A.; Pacifici, D.; Atwater, H. A. *Nano Lett.* **2008**, *8*, 4391–4397.
- (36) Abass, A.; Shen, H.; Bienstman, P.; Maes, B. *J. Appl. Phys.* **2011**, *109*, 023111.
- (37) Munday, J. N.; Atwater, H. A. *Nano Lett.* **2010**, *11*, 2195–2201.
- (38) Pala, R. A.; White, J.; Barnard, E.; Liu, J.; Brongersma, M. L. *Adv. Mater.* **2009**, *21*, 3504–3509.
- (39) Tao, A.; Sinsermsuksakul, P.; Yang, P. *Nat. Nanotechnol.* **2007**, *2*, 435–440.